Kinetic-energy release of fragments from electron-impact dissociation of the molecular hydrogen ion and its isotopologues

Liam H. Scarlett,[1,*] Mark C. Zammit,[1,2,†] Dmitry V. Fursa,[1] and Igor Bray[1]

[1]*Curtin Institute for Computation and Department of Physics, Astronomy and Medical Radiation Sciences, Curtin University, Perth, Western Australia 6102, Australia*

[2]*Theoretical Division, Los Alamos National Laboratory, Los Alamos, New Mexico 87545, USA*

(Received 28 April 2017; published 18 August 2017)

We calculate the kinetic-energy release distributions of fragments produced for electron-impact dissociation of the vibrationally excited molecular hydrogen ion H_2^+ and its isotopologues D_2^+ and T_2^+. Here we apply the adiabatic-nuclei convergent close-coupling method and compare results with several different methods, including the δ approximation. Results are presented for a number of dissociative excitation transitions and dissociative ionization as a function of the initial vibrational state of the molecule. We confirm that the square root approximation is a good approximation for the adiabatic-nuclei kinetic-energy release cross sections of H_2^+. Agreement with experiment, where available, is good.

DOI: 10.1103/PhysRevA.96.022706

I. INTRODUCTION

Electron-impact dissociative ionization or excitation of molecular ions

$$e^- + AB^+ \rightarrow A^+ + B^+ + 2e^- \quad (1)$$

$$\rightarrow A^+ + B + e^- \quad (2)$$

$$\rightarrow A + B^+ + e^- \quad (3)$$

produces fragments with a kinetic-energy release (KER) distribution. These collision processes are among the most important for determining fusion and low-temperature plasma dynamics and properties and can also be used to control plasma conditions [1,2]. Information about the KER distribution is used to determine energy deposition and reactivity in the respective media, which is important in the fields of radiotherapy [3–6] and astrophysics [7].

The KER distributions correspond to excitations to the vibrational continuum and are the fragment single-differential cross sections. Many experimental measurements of the KER cross sections have been used to extract scattering cross sections [8–18], identify dissociative processes [8–18], and determine experimental conditions [18–20], molecular structure [21,22], and collision dynamics [21]. The KER cross sections can be extracted from a complete close-coupling calculation that includes all degrees of freedom (electronic, vibrational, and rotational). Several theoretical methods have been utilized to give an approximate KER cross section. Stibbe and Tennyson [23] derived a form of the adiabatic-nuclei cross section for vibrationally resolved excitations, utilizing electronic T-matrix elements. A modified form of this T-matrix approach, and the square root approximation, were implemented by Zammit *et al.* [24] in the study of positron-H_2 scattering.

The molecular hydrogen ion H_2^+ is the most convenient starting point for developing a KER model, as it is the simplest molecular system and still exhibits all processes (1)–(3). It is commonly present in fusion and astrophysical plasmas where its dissociative processes play an important role in determining plasma properties.

There has been a limited number of theoretical calculations of the H_2^+ KER cross sections, likely due to the complexity of calculating accurate collision data for molecules. Dunn [25] utilized the δ (reflection) approximation and the first Born approximation electronic excitation cross sections of Peek [26] to calculate H_2^+ KER cross sections that are valid only in the high incident electron energy limit. El Ghazaly *et al.* [18] used the more accurate square root approximation, with excitation cross sections derived from the oscillator strengths of Ramaker and Peek [27], yielding results in reasonable agreement with experiment. The lack of theoretical KER cross sections calculated using accurate collision data motivates the present work. Recently, Zammit *et al.* [28,29] applied the convergent close-coupling (CCC) method to model electron collisions with H_2^+ and its isotopologues. The CCC results were in good agreement with measurements of proton-production and dissociative ionization cross sections. Utilizing these results, here we calculate the KER cross sections using the T-matrix, square root, and δ approximation methods and compare their agreement with each other and with the measurements of El Ghazaly *et al.* [18]. Atomic units are used throughout this paper unless specified otherwise.

II. THEORY

The molecular CCC method for e^--H_2^+ scattering has been described in detail by Zammit *et al.* [28–30]. Here we give a brief overview. The theory is formulated in spherical coordinates, with the origin at the geometrical center of the nuclei. Calculations have been performed in the adiabatic-nuclei approximation [30,31]. This approximation applies the Born-Oppenheimer approximation to the total scattering wave function, effectively reducing the electron-molecule scattering problem to one involving only the electronic degrees of freedom. We formulate the scattering system electronic Schrödinger equation in the body (molecule fixed) frame at a fixed internuclear distance R and substitute a close-

*liam.scarlett@student.curtin.edu.au

†mzammit@lanl.gov

coupling expansion constructed from a set of target electronic (Sturmian) pseudostates. Substitution of this expansion into the Schrödinger equation leads to a set of momentum-space Lippmann-Schwinger close-coupling equations for the electronic T matrix. These equations are solved via a K-matrix formulation, which enforces unitarity. Expanding the projectile wave function in partial waves allows one to solve the close-coupling equations per partial-wave of total (electronic) orbital angular momentum projection M, spin S, and parity Π. The electronic body-frame T-matrix elements are then transformed to the laboratory frame using standard techniques [30,31]. Here we perform (semiclassical) orientation averaging of the differential and integrated cross sections [32], which is equivalent to summing over all rotational excitations from the rotational ground state, analytically. By performing calculations at many internuclear distances R, information of the nuclear motion (KER, rotational, and vibrational excitations) can be obtained via postprocessing of the electronic fixed-nuclei T-matrix elements.

Fixed-nuclei electronic excitation cross sections in the total spin channel S are obtained from the electronic T-matrix elements $T^S_{fL_fM_f,iL_iM_i}(R;E_{\rm in})$ for electronic transitions $i \to f$, via

$$\sigma^S_{f,i}(R;E_{\rm in}) = 4\pi^3 \frac{q_f(R)}{q_i} \sum_{\substack{L_f,L_i \\ M_f,M_i}} \left|T^S_{fL_fM_f,iL_iM_i}(R;E_{\rm in})\right|^2, \tag{4}$$

where the projectile momenta are calculated from the incident energy $E_{\rm in}$ and excitation energy $\varepsilon_{f,i}$:

$$q_f(R) = \sqrt{2[E_{\rm in} - \varepsilon_{f,i}(R)]}, \tag{5}$$

$$q_i = \sqrt{2E_{\rm in}}. \tag{6}$$

The spin-averaged cross sections are given by

$$\sigma_{f,i} = \sum_S \frac{2S+1}{4} \sigma^S_{f,i}. \tag{7}$$

The T-matrix elements are solved for a sufficient number of partial waves to achieve convergence with the use of an analytic Born subtraction technique [28,33]. Cross sections for the dissociative ionization (DI) process (1) are calculated by summing over all positive-energy states

$$\sigma_{{\rm DI},i}(R;E_{\rm in}) = \sum_{\epsilon_f>0} \sigma_{f,i}(R;E_{\rm in}), \tag{8}$$

where ϵ_f is the energy of state f.

For the case of the H_2^+ molecule, practically all excited electronic state potential-energy curves are repulsive [34–36] and hence all electronic excitations lead to dissociation. In Fig. 1 we present the potential-energy curves obtained from the spherical formulation, as a function of internuclear separation. We compare with the exact results obtained using a spheroidal formulation of the electronic H_2^+ problem [37]. In spheroidal coordinates, the H_2^+ structure problem is separable and can be solved analytically. The energies obtained from the spherical structure model are in excellent agreement with the exact results for the higher-energy states that are more hydrogenic.

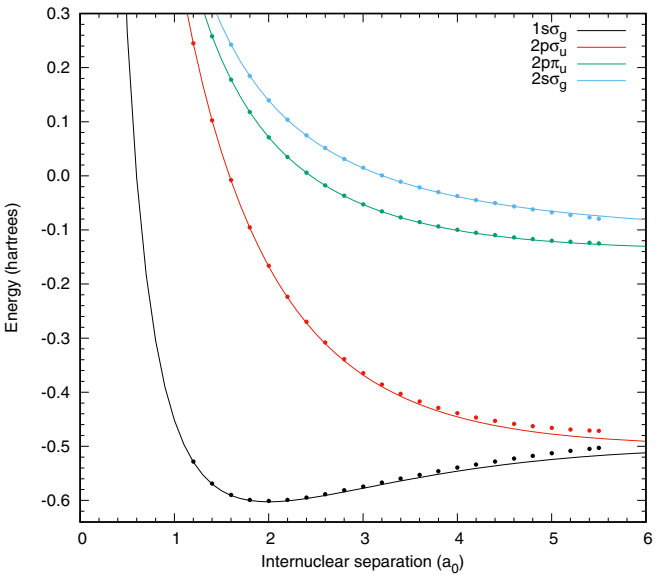

FIG. 1. Potential-energy curves of the $1s\sigma_g$, $2p\sigma_u$, $2p\pi_u$, and $2s\sigma_g$ states obtained from the spherical (points) and spheroidal (lines) electronic structure calculations.

The two lowest-energy states are more difficult to describe with single-center orbitals, particularly at larger internuclear separations. The spherical calculations were driven to convergence near the equilibrium separation $R = 2.0a_0$ and are sufficiently accurate for scattering calculations up to $R = 5.5a_0$. We have implemented an extrapolation technique wherever scattering data are required at larger R.

Following the adiabatic-nuclei (AN) approximation [31], cross sections for transitions between vibrational bound states $\chi_{nv_n}(R)$ and continuum states $\chi_n(R;E_{\rm k})$, where $E_{\rm k}$ is the fragment kinetic energy, summed over all final rotational states

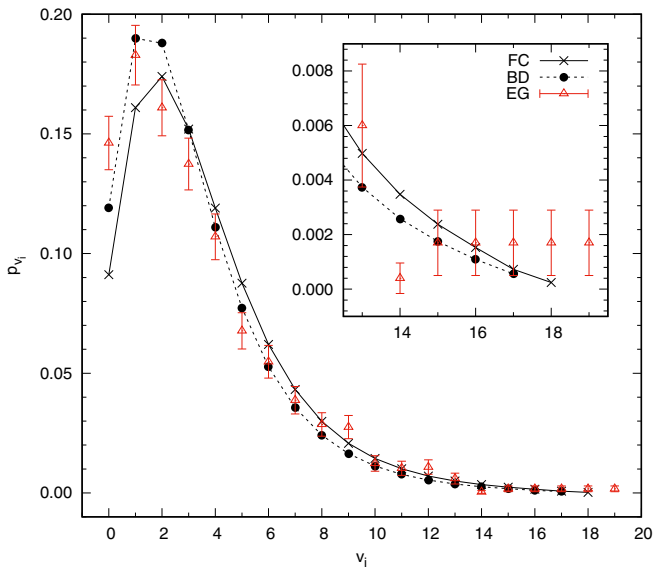

FIG. 2. Vibrational weights p_{v_i} of H_2^+: FC factors [28], BD weights [40], and EG weights [18], as a function of vibrational state number v_i.

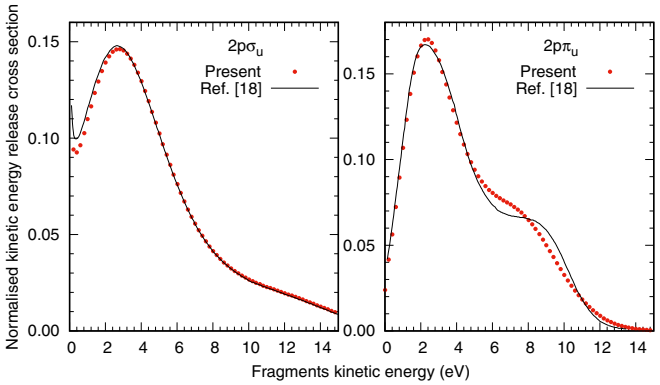

FIG. 3. Comparison of the $2p\sigma_u$ (left) and $2p\pi_u$ (right) BD-weighted normalized KER cross sections with the model calculations of El Ghazaly *et al.* [18]. These results have been calculated using the same approximate excitation cross sections used by El Ghazaly *et al.* [18] (parabolic for $2p\sigma_u$ and flat for $2p\pi_u$).

J_f can be expressed in the form

$$\frac{d\sigma^S_{f,iv_i}}{dE_k} = 4\pi^3 \sum_{\substack{L_f,L_i \\ M_f,M_i}} \left| \langle \chi_f | \sqrt{\frac{q_f}{q_i}} T^S_{fL_fM_f,iL_iM_i} | \chi_{iv_i} \rangle_R \right|^2. \quad (9)$$

The bound and continuum vibrational wave functions $\chi(R)$ satisfy the Schrödinger equation

$$\frac{d^2\chi}{dR^2} + 2\mu\left(E_k - \frac{J(J+1) - m_n^2}{2\mu R^2} - \varepsilon_n(R)\right)\chi = 0, \quad (10)$$

where $\varepsilon_n(R)$ is the interaction potential between fragments, i.e., the electronic state potential energy minus the dissociation energy, J is the rotational quantum number, m_n is the orbital angular momentum projection of the electronic state n, and μ is the reduced mass of the dissociative products. For H_2^+, μ is half the proton mass. We remove the explicit dependence of the vibrational functions on J, by taking $J = 0$ for $m_n = 0$ and $J = 1$ for $m_n = \pm 1$. For the calculation of the continuum wave functions we use the accurate potential-energy curves obtained from the spheroidal formulation [37]. The energy normalized continuum functions are obtained by solving Eq. (10) using the Numerov method. They have the asymptotic form

$$\lim_{R\to\infty} \chi_f(R; E_k) = \sqrt{\frac{2\mu}{k\pi}} \sin(kR + \delta) \quad (11)$$

and satisfy the property

$$\int_0^\infty \chi_f(R; E_k)\chi_f(R; E_k')dR = \delta(E_k - E_k'). \quad (12)$$

The bound vibrational wave functions $\chi_{nv_n}(R)$ are obtained via diagonalization of the ground electronic state Hamiltonian in a basis of nuclear functions

$$\phi_n(\vec{R}) = \frac{1}{R}\varphi_{nJ}(R)Y_{J m_J}(\hat{\vec{R}}), \quad (13)$$

where φ_{nJ} are the Laguerre basis functions as described in [28,29]. Here we utilize the $1s\sigma_g$ potential-energy curve from

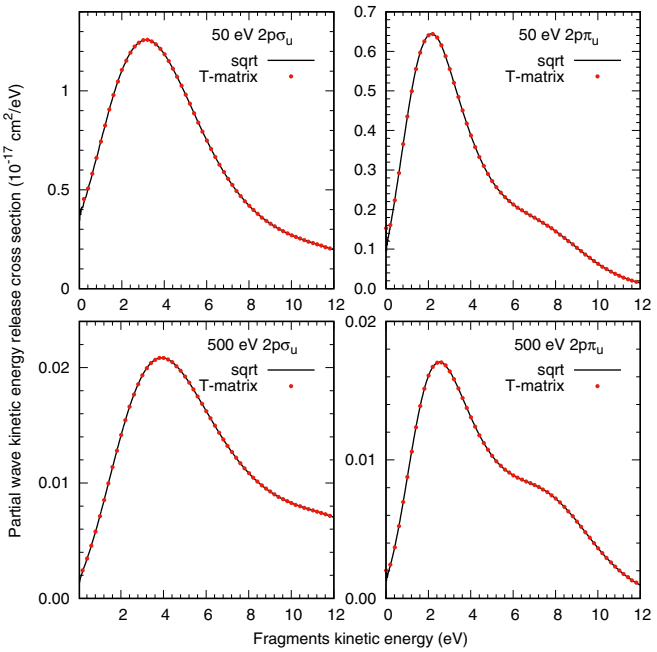

FIG. 4. The BD-weighted partial wave KER cross sections for the $2p\sigma_u$ and $2p\pi_u$ states at 50- and 500-eV incident energies, calculated using the square root approximation and T-matrix method.

Wolniewicz and Poll [38]. The closure property

$$\sum_{v_n} \chi_{nv_n}(R)\chi_{nv_n}(R') + \int_0^\infty \chi_n(R; E_k)\chi_n(R'; E_k)dE_k = \delta(R - R') \quad (14)$$

is used to sum over all final vibrational states to obtain the AN cross section

$$\sigma_{f,iv_i} = \langle \chi_{iv_i} | \sigma_{f,i} | \chi_{iv_i} \rangle_R, \quad (15)$$

which describes scattering from the v_i vibrational level of the initial electronic state i to all rovibrational levels of the final electronic state f.

Stibbe and Tennyson [23] derived a form of the KER cross section that requires the use of off-shell T-matrix elements to account for the varying proportions in which the dissociation energy can be split among the dissociation products and the outgoing electron. By neglecting the differences in the vibrational energy levels the KER cross sections of [23] can be simplified to the form of Eq. (9), where only on-shell T-matrix elements are used. We hereafter refer to this method of calculation as the T-matrix method.

A. Square root approximation

Evaluation of Eq. (9) is computationally expensive due to the large number of numerical integrations that must be performed. Following El Ghazaly *et al.* [18], we replace the constants and the T-matrix elements in Eq. (9) with the square root of the electronic excitation cross section at incident electron energy E_{in}:

$$\frac{d\sigma_{f,iv_i}}{dE_k} = |\langle \chi_f | \sqrt{\sigma_{f,i}} | \chi_{iv_i} \rangle_R|^2. \quad (16)$$

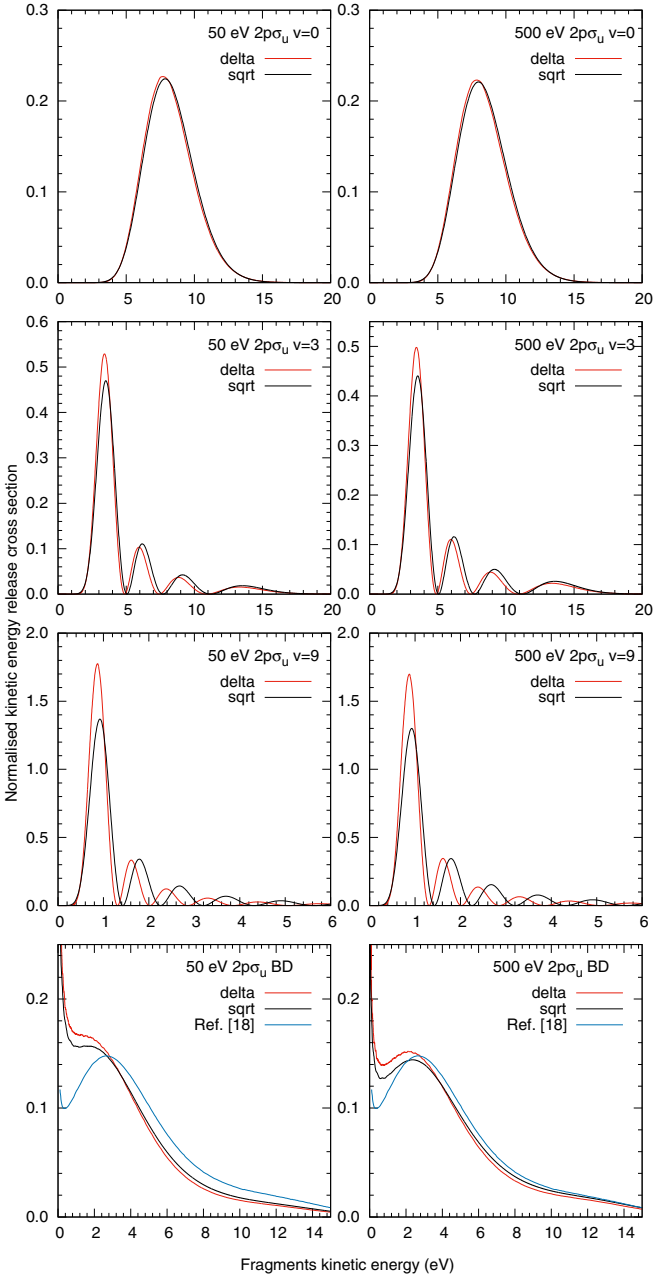

FIG. 5. Normalized KER cross sections of the $2p\sigma_u$ state of H_2^+ at $E_{in} = 50$ and 500 eV. The first three rows present scattering on the $v_i = 0$, 3, and 9 states and the final row presents the BD-weighted sum over the $v_i = 0$–18 states, compared with the model calculations of El Ghazaly *et al.* [18].

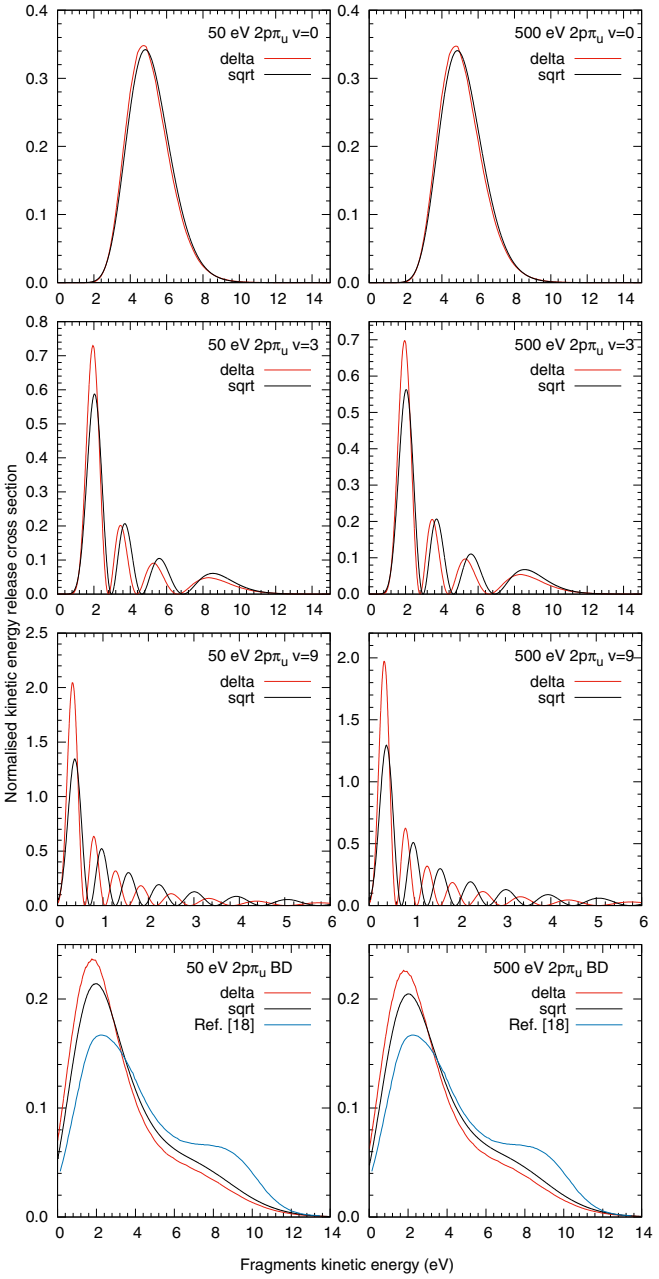

FIG. 6. Same as in Fig. 5 but for the $2p\pi_u$ state of H_2^+.

This form requires only a single integration and makes KER calculations much faster. Construction of the DI KER cross section in the square root approximation formally requires a summation over positive-energy states as in Eq. (8). However, due to the complexity of resolving R-dependent cross sections for specific states when their respective potential-energy curves cross, we instead calculate the DI KER cross section via

$$\frac{d\sigma_{\mathrm{DI},iv_i}}{dE_k} = |\langle \chi_f | \sqrt{\sigma_{\mathrm{DI},i}} | \chi_{iv_i} \rangle_R|^2. \quad (17)$$

The square root technique was implemented by Zammit *et al.* [24] to obtain vibrationally resolved excitation cross sections for positron scattering on H_2, yielding results practically identical to those obtained with the T-matrix method. El Ghazaly *et al.* [18] constructed model e^--H_2^+ KER distributions by replacing the excitation cross sections in Eq. (16) with simple R dependences obtained from photonic excitations of H_2^+ and compared with their experimental measurements with reasonable success.

B. The δ approximation

The integrand in Eq. (9) is highly oscillatory except in the vicinity of the continuum function's classical turning point R_c. Accordingly, the integral can be approximated by the

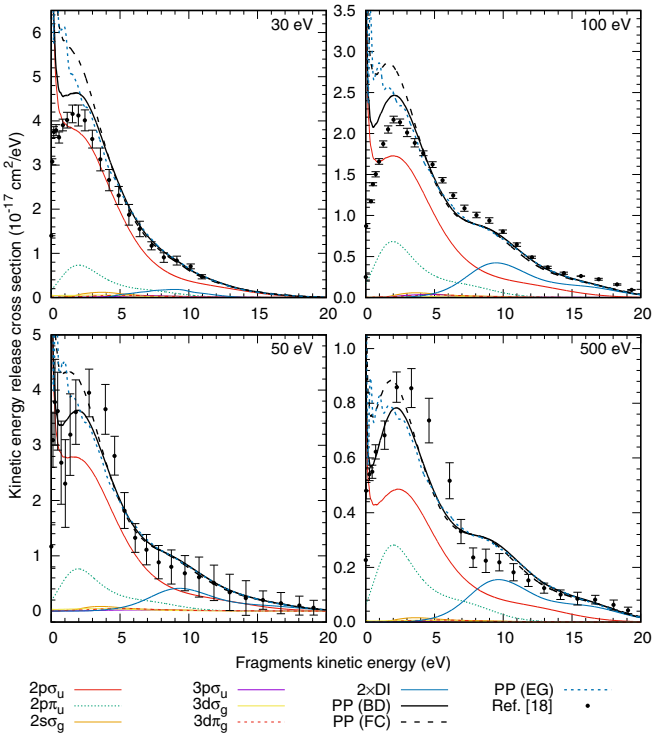

FIG. 7. The KER cross sections of the $2p\sigma_u$, $2p\pi_u$, $2s\sigma_g$, $3p\sigma_u$, $3d\sigma_g$, and $3d\pi_g$ states and DI for H_2^+ at 30-, 50-, 100-, and 500-eV incident electron energies, calculated using the square root approximation. The individual channels presented here were calculated using BD weights. The FC-, BD-, and EG-weighted PP KER cross sections are also presented in comparison with the measurements of El Ghazaly *et al.* [18].

contribution at this point by replacing the continuum wave function with an appropriately normalized δ function

$$\chi_{f v_f}(R;E_k) = \frac{1}{\sqrt{|d\varepsilon_f/dR|}}\delta(E_k - \varepsilon_f(R)). \quad (18)$$

Gislason [39] developed an approximate calculation of the overlap $\langle\chi_f|\chi_{iv_i}\rangle$, by expanding the effective potential $\varepsilon_f(R)$ and the bound vibrational wave function $\chi_{iv_i}(R)$ about R_c. By taking just the first-order term they recover the correctly normalized δ approximation. The normalization constant can also be derived by requiring the continuum functions to satisfy

$$\int_0^\infty |\langle\chi_f|\chi_{iv_i}\rangle|^2 dE = 1. \quad (19)$$

In the δ approximation the KER cross section becomes

$$\frac{d\sigma_{f,iv_i}}{dE_k} = \frac{1}{|d\varepsilon_f/dR|}\delta(E_k - \varepsilon_f(R))\sigma_{f,i}(R)|\chi_{iv_i}(R)|^2. \quad (20)$$

C. Vibrational weighting

Many scattering measurements have been taken with H_2^+ populated in a range of vibrationally excited states [40]. Hence cross sections need to be weighted according to a vibrational distribution

$$\frac{d\tilde{\sigma}_{f,i}}{dE_k} = \sum_{v_i} p_{v_i}\frac{d\sigma_{f,iv_i}}{dE_k}, \quad (21)$$

where p_{v_i} are normalized weights for the distribution of initial target vibrational levels

$$\sum_{v_i} p_{v_i} = 1. \quad (22)$$

We perform calculations using the Franck-Condon (FC) factors [28,29,41] and the vibrational populations measured by von Busch and Dunn [40] and El Ghazaly *et al.* [18], which we refer to hereafter as BD and EG weights, respectively. We present these vibrational distributions in Fig. 2.

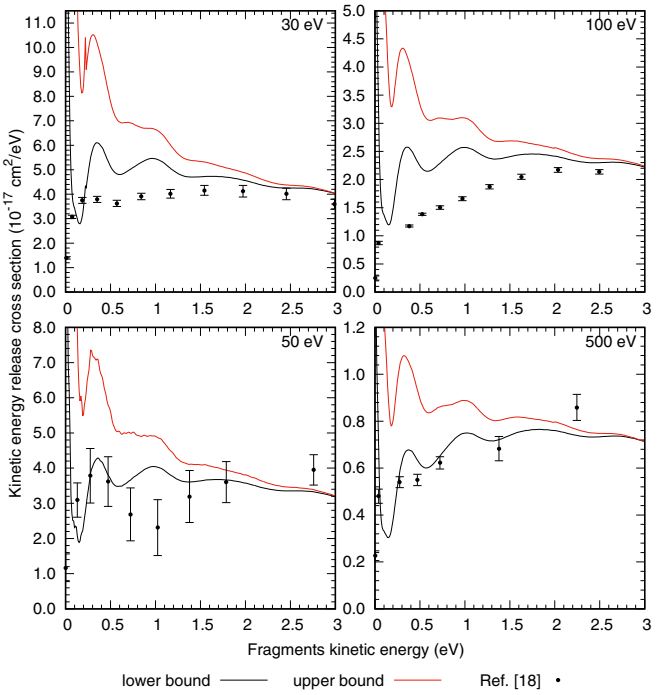

FIG. 8. Upper and lower bounds on the EG-weighted PP KER cross section for 30-, 50-, 100-, and 500-eV incident electrons. The results are compared with the measurements of El Ghazaly *et al.* [18].

D. Summation over electronic states

Measurements of the H_2^+ KER cross sections contain contributions from all open electronic transitions. El Ghazaly *et al.* [18] measured KER cross sections for H_2^+ by the detection of protons. When they are integrated over E_k, the vibrationally weighted proton-production (PP) cross section $\tilde{\sigma}_{PP} = \tilde{\sigma}_{DE} + 2\tilde{\sigma}_{DI}$ is obtained. Here DE designates the dissociative excitation (2) and (3) processes. To compare with experiment we must construct the PP KER cross section

$$\frac{d\tilde{\sigma}_{PP}}{dE_k} = \sum_{\epsilon_f<0}\frac{d\tilde{\sigma}_{f,i}}{dE_k} + 2\frac{d\sigma_{DI,i}}{dE_k}. \quad (23)$$

It can be shown that for each of the three methods detailed above, integration of the vibrationally weighted KER cross section (21) over E_k yields the vibrationally weighted AN

TABLE I. Weights measured by El Ghazaly *et al.* [18] for the initial vibrational states v_i of H_2^+. Also presented are the upper and lower bounds we placed on the EG weights by taking the bounds given by experimental uncertainty (see Fig. 2) and renormalizing to satisfy Eq. (22).

		Renormalized bounds	
v_i	EG weights [18]	Upper	Lower
0	0.14620	0.14258	0.15063
1	0.18290	0.17703	0.19010
2	0.16090	0.15639	0.16642
3	0.13740	0.13429	0.14120
4	0.10700	0.10560	0.10870
5	0.06770	0.06822	0.06705
6	0.05480	0.05584	0.05351
7	0.03870	0.04027	0.03677
8	0.02860	0.03038	0.02640
9	0.02750	0.02930	0.02528
10	0.01230	0.01407	0.01011
11	0.01030	0.01201	0.00819
12	0.01080	0.01253	0.00867
13	0.00600	0.00748	0.00418
14	0.00040	0.00870	0.00000
15	0.00170	0.00263	0.00056
16	0.00170	0.00263	0.00056
17	0.00170	0.00263	0.00056
18	0.00170	0.00263	0.00056
19	0.00170	0.00263	0.00056

electronic excitation cross section

$$\tilde{\sigma}_{f,i} = \sum_{v_i} p_{v_i} \sigma_{f,iv_i}, \tag{24}$$

where σ_{f,iv_i} is given in Eq. (15). Hence, integration of the PP KER cross section (23) over E_k yields $\tilde{\sigma}_{PP}$ as required for comparison with El Ghazaly *et al.* [18]. Note that the DI cross sections [18,42] are an order of magnitude lower than the PP cross sections and are smaller than the experimental error bars of $\tilde{\sigma}_{PP}$ [34,35,43,44]. Hence the results of DE, total inelastic, and PP cross sections can be compared with each other reasonably well. Despite the small contribution to $\tilde{\sigma}_{PP}$, at some fragment energies the DI process makes the dominant contribution to the PP KER cross sections.

III. RESULTS

KER calculations of e^--H_2^+ scattering have been performed for incident energies from 30 to 500 eV, using the δ, square root, and T-matrix methods as detailed in Sec. II. We calculate KER cross sections for excitation to the $2p\sigma_u$, $2p\pi_u$, $2s\sigma_g$, $3p\sigma_u$, $3d\sigma_g$, and $3d\pi_g$ states, as well as the DI KER cross section, and compare the various methods. The discrete electronic states with even larger energies than those mentioned above make negligible contributions to the PP KER cross sections and hence are not presented here [28]. El Ghazaly *et al.* [18] provided measurements of H_2^+ and D_2^+ KER cross sections for $E_{in} = 30, 50, 100$, and 500 eV. Relative H_2^+ KER measurements were also presented by Caudano and Delfosse [45] and when scaled to the measurements of El Ghazaly *et al.* [18] they were in good agreement. For this reason we omit comparison with Caudano and Delfosse [45] and compare our results with the more precise measurements and model calculations of El Ghazaly *et al.* [18].

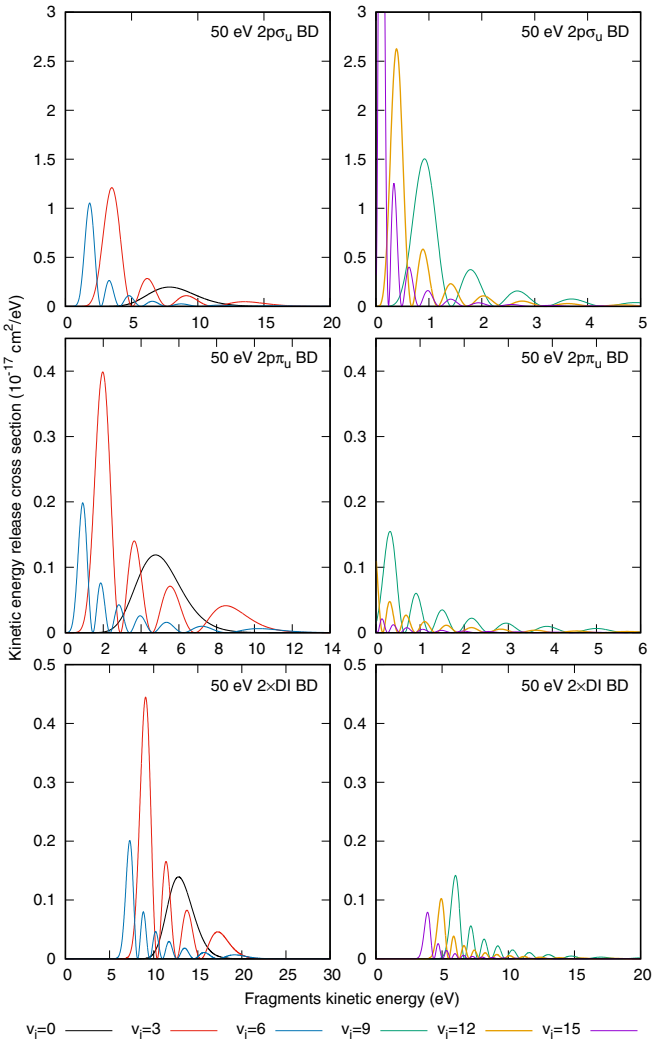

FIG. 9. The BD-weighted $2p\sigma_u$ and $2p\pi_u$ and DI KER cross sections for 50-eV electrons scattering on individual vibrational levels of H_2^+, demonstrating that the low-lying vibrational states make the largest contribution at high E_k.

A. Comparison of methods

El Ghazaly *et al.* [18] calculated BD-weighted KER cross sections using Eqs. (16) and (21), by assuming a parabolic $\sigma_{f,i}(R)$ with respect to R for the $1s\sigma_g \rightarrow 2p\sigma_u$ transition and a flat $\sigma_{f,i}(R)$ for the $1s\sigma_g \rightarrow 2p\pi_u$ transition. In Fig. 3 we present our BD-weighted KER cross sections for the $2p\sigma_u$ and $2p\pi_u$ states using the same approximations. These results are normalized to have unit area under the curve to allow for comparison with [18]. The agreement of our calculations with the El Ghazaly *et al.* [18] model is very good. The minor discrepancy for the $2p\pi_u$ results is due to the use of different potential-energy curves.

From here onward we utilize the collision data calculated by Zammit *et al.* [28,29]. To make a direct comparison between the square root and T-matrix methods, we calculate the partial

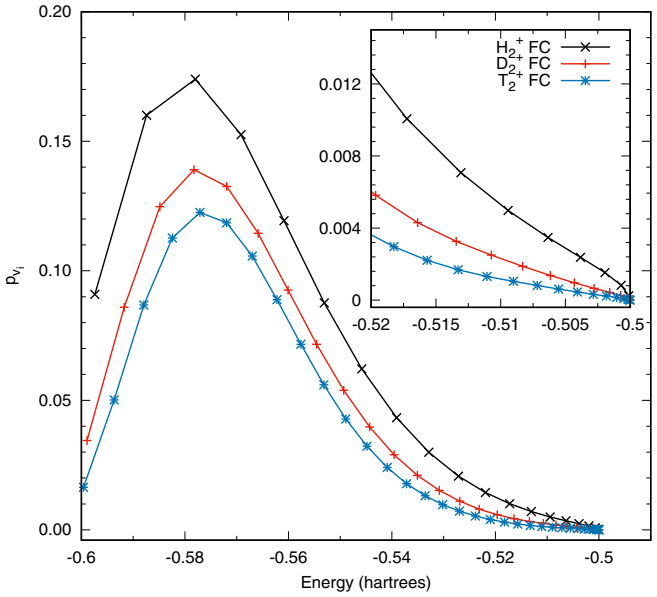

FIG. 10. The FC factors p_{v_i} [28] for H_2^+, D_2^+, and T_2^+ as a function of vibrational state energy.

wave KER cross section using both methods without analytic Born subtraction. We present these calculations at $E_{\rm in} = 50$ and 500 eV for the BD-weighted $2p\sigma_u$ and $2p\pi_u$ states in Fig. 4. We find excellent agreement between the two methods of calculation, except minor discrepancies at very low $E_{\rm k}$. The level of agreement between the two methods at $E_{\rm in} = 30$ and 100 eV is the same. Similar agreement between the two methods was also found in the calculation of vibrationally resolved excitations for positron-H_2 scattering by Zammit *et al.* [24]. As the use of the square root method is much simpler computationally, we will use it in what follows to compare with the δ approximation and with experiment.

In Fig. 5 we present the normalized KER cross sections for excitation to the $2p\sigma_u$ state of H_2^+ by 50- and 500-eV electrons scattering on the $v_i = 0,3,9$ vibrational states and the BD-weighted sum over the $v_i = 0$–18 states. For each, the square root and δ approximations are compared and the BD-weighted results are also compared with the model calculations of El Ghazaly *et al.* [18]. The δ and square root approximation results are in good agreement for the $v_i = 0$ ground state, but the discrepancy becomes greater for highly excited vibrational states. The cumulative effect is that the δ approximation adequately reproduces the square root results at higher $E_{\rm k}$, where the largest contribution comes from lower vibrational states, but fails at low $E_{\rm k}$ where the largest contribution is from higher vibrational states. Our calculations are in better agreement with the El Ghazaly *et al.* [18] model calculations at 500 eV than at 50 eV, because their approximate excitation cross sections are valid only in the high-$E_{\rm in}$ limit. The disagreement at $E_{\rm in} = 50$ eV demonstrates the importance of using accurate collision data in the KER calculations. In Fig. 6 the same results are presented for the $2p\pi_u$ state. The comparisons between the δ and square root methods are the same as those described for the $2p\sigma_u$ state. In addition, we have verified that the square root and T-matrix methods are in excellent agreement for the $2p\sigma_u$ and $2p\pi_u$ individual vibrational level partial-wave KER cross sections. The larger discrepancy between our results and the El Ghazaly *et al.* [18] model for the $2p\pi_u$ state than for the $2p\sigma_u$ state is likely due to our use of different potential-energy curves. The BD-weighted $2p\sigma_u$ results display a peak near the origin that comes from the highest excited vibrational levels. The largest contribution to the low-$E_{\rm k}$ KER cross section comes from large values of R, which are sampled only by the higher vibrational levels. At these internuclear separations the $2p\sigma_u$ state becomes degenerate with the ground $1s\sigma_g$ state, resulting in an increased excitation probability and therefore a larger KER cross section. This effect is not present in the $2p\pi_u$ results because of the higher asymptotic energy of this state.

B. Proton-production KER cross sections

In Fig. 7 we present the BD-, EG-, and FC-weighted PP KER cross sections for $E_{\rm in} = 30$, 50, 100, and 500 eV and compare with the experimental measurements of El Ghazaly *et al.* [18]. We also show the individual BD-weighted KER cross sections of the $2p\sigma_u$, $2p\pi_u$, $2s\sigma_g$, $3p\sigma_u$, $3d\sigma_g$, and $3d\pi_g$ states of H_2^+ as well as the DI KER cross section. All calculations have been performed using the square root approximation, which we confirmed above to be a very good approximation of the T-matrix method. These figures illustrate the relative contributions of each state to the PP KER cross section. As noted by El Ghazaly *et al.* [18] and in our previous investigations [28,29] into e^--H_2^+ scattering, the $2p\sigma_u$ state makes the largest contribution, followed by the $2p\pi_u$ state and DI. The remaining states make very little contribution to the PP KER cross section. The PP KER cross sections calculated using the different vibrational weights are in good agreement with each other for $E_{\rm k}$ greater than 4 eV, but are in significant disagreement at lower $E_{\rm k}$, demonstrating the sensitivity of the low-$E_{\rm k}$ KER cross section to the choice of vibrational distribution. At each $E_{\rm in}$ our results are in good qualitative agreement with those of El Ghazaly *et al.* [18] and at $E_{\rm in} = 50$ eV our results are in good quantitative agreement.

El Ghazaly *et al.* [18] extracted DI cross sections as a function of incident electron energy from the high-fragment-energy tail of the KER cross sections, reasoning that the DI KER cross section extends well beyond the DE processes. Here, however, we have demonstrated that the $2p\sigma_u$ state makes a significant contribution to the high-fragment-energy tail. At 30-eV incident energy the $2p\sigma_u$ state makes the dominant contribution and at 500 eV it still accounts for approximately one-third of the high-fragment-energy tail. The underlying CCC DI cross sections used in this work were compared [28] with the measurements of El Ghazaly *et al.* [18] and Peart and Dolder [42]. The CCC cross sections are in good agreement with those of Peart and Dolder [42], but those of El Ghazaly *et al.* [18] are substantially higher, likely due to the contribution from the $2p\sigma_u$ state.

In Fig. 8 we present upper and lower bounds for the EG-weighted PP KER cross sections, constructed by weighting the cross sections with the renormalized maximum and minimum values of the EG weights shown in Fig. 2. The EG weights, along with the renormalized bounds, are presented in Table I. The upper bound weights have a larger contribution from the higher vibrational levels than the lower bound weights. The

uncertainty in the vibrational distribution has no significant effect in the region $E_k > 3$ eV, but for $E_k < 3$ eV it has a strong effect. At all four incident energies the EG-weighted PP KER cross sections are in better agreement with those of El Ghazaly *et al.* [18] when we take the lower bound of the vibrational distribution. In particular, the agreement for $E_{in} =$ 50 and 500 eV is very good. This demonstrates the sensitivity of the results to uncertainties in the vibrational distribution. Our results suggest that the actual vibrational population in the experiment of El Ghazaly *et al.* [18] had smaller weights for the highest vibrational states than what was reported.

In Fig. 9 we present the BD-weighted $2p\sigma_u$ and $2p\pi_u$ and DI KER cross sections for 50-eV electrons scattering on individual vibrational levels of H_2^+. This figure demonstrates that the low-lying vibrational states make the largest contribution to the vibrationally summed KER cross section at high E_k. The very good agreement of our PP KER cross sections with those of El Ghazaly *et al.* [18] at high E_k (see Fig. 7) indicates that we have calculated [28] accurate collision data for both DE and DI from the low-lying vibrational states. This confirms that these results can serve as a benchmark calculation.

C. The isotopologues D_2^+ and T_2^+

In the Born-Oppenheimer approximation, the isotopologues D_2^+ and T_2^+ have potential-energy curves and electronic excitation cross sections identical to those of H_2^+. Hence, to calculate KER cross sections for these isotopologues, all that is required is to obtain the bound vibrational levels, using the appropriate reduced mass μ for D_2^+ or T_2^+ (half the mass of a deuteron and a triton, respectively) in Eq. (10).

The vibrational levels become more closely spaced in energy as μ is increased, resulting in a greater number of bound states. In Fig. 10 we present the FC factors [28] for H_2^+, D_2^+, and T_2^+, as a function of the vibrational state energy.

The low-E_k spike present in the H_2^+ results is due to the contribution from vibrational states $v = 15$ and above. These levels have energies greater than -0.505 hartree (see Fig. 10). Summing the FC factors for vibrational levels with energies greater than -0.505 yields 0.005 for H_2^+, 0.003 for D_2^+, and 0.001 for T_2^+. Therefore, the KER cross sections for the vibrational levels that contribute to the low-E_k spike are weighted less for D_2^+ and T_2^+. As for H_2^+, it is likely that the FC distribution assumed here has a larger weighting on the higher vibrational states than what is produced in experiment. This is evident from the behavior of the measurements at low E_k.

In Fig. 11 we present the FC-weighted PP KER cross sections for H_2^+ and compare them with the deuteron-production (DP) and triton-production (TP) KER cross sections for D_2^+ and T_2^+, respectively. The results for all three isotopologues are practically the same, except in the region $E_k \leqslant 2$ eV. This is due to the fact that, in the Born-Oppenheimer approximation, the isotopologues are distinguished only by their vibrational levels and populations, which do not have a strong effect on the KER cross sections except at low E_k. The spike near the origin is less pronounced for the heavy isotopologues than for H_2^+, due to the decrease in population of the high-energy vibrational levels. In Fig. 12 we compare the $E_{in} = 100$ eV D_2^+ DP KER

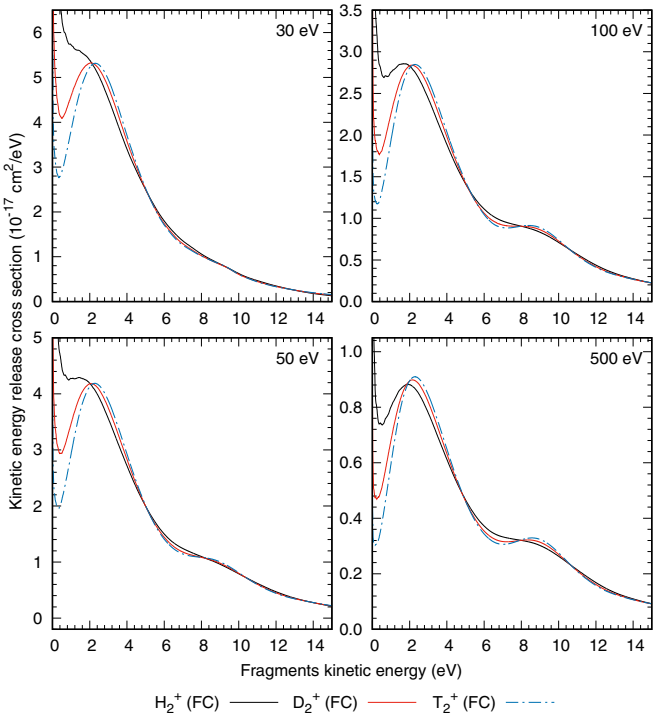

FIG. 11. The FC-weighted PP KER cross sections for 30-, 50-, 100-, and 500-eV electrons incident on H_2^+, compared with the DP and TP KER cross sections for D_2^+ and T_2^+, respectively.

cross section with the D_2^+ measurements of El Ghazaly *et al.* [18]. Although the present H_2^+ and D_2^+ KER results are very similar away from low E_k as expected, we have a worse level of agreement with experiment for D_2^+ than we did for the

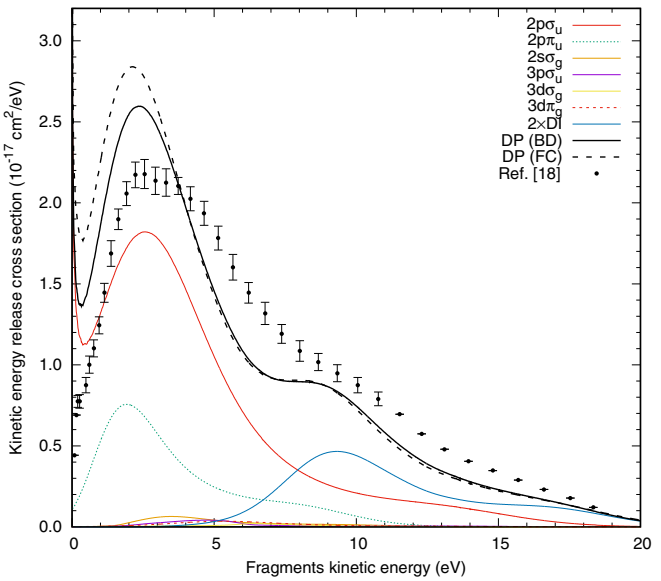

FIG. 12. The KER cross sections of the $2p\sigma_u$, $2p\pi_u$, $2s\sigma_g$, $3p\sigma_u$, $3d\sigma_g$, and $3d\pi_g$ states and DI for D_2^+ at 100-eV incident electron energy, calculated using the square root approximation. The individual channels presented here were calculated with BD weights. The FC- and BD-weighted DP KER cross sections are also presented in comparison with the measurements of El Ghazaly *et al.* [18].

H_2^+ results presented in Fig. 7. The D_2^+ measurements of El Ghazaly *et al.* [18] are higher than the H_2^+ measurements in the high-E_k region where our calculations show they should be in agreement. As shown previously, the PP KER cross sections at large E_k are relatively insensitive to the assumed vibrational distributions (Figs. 7 and 8), hence the discrepancy between our D_2^+ results and experiment is unlikely to be (primarily) due to the assumed FC distribution. The difference between the H_2^+ and D_2^+ measurements deserves further investigation.

IV. CONCLUSION

We have calculated KER cross sections for electron scattering on H_2^+ in the incident energy range from 30 to 500 eV. We have compared calculations using the T-matrix method, the δ (reflection) approximation, and the square root approximation. We find that the δ approximation, which replaces the continuum wave function with a δ function, is in poor agreement with the other methods except when scattering from the ground vibrational state. The T-matrix and square root methods are in excellent agreement for the two most important dissociative excitations ($1s\sigma_g \rightarrow 2p\sigma_u$ and $1s\sigma_g \rightarrow 2p\pi_u$) over the range of incident energies that we have performed calculations for.

We have demonstrated that our results reproduce the model calculations of El Ghazaly *et al.* [18] when we implement the same approximations and find good agreement with their experimental data when we perform calculations using accurate collision data calculated using the molecular CCC method [28,29]. The uncertainty in the population of the high vibrational states in the experiment of El Ghazaly *et al.* [18] could be responsible for the moderate agreement of their results with our calculations.

We have shown that in the low-E_k region, the KER cross section is highly sensitive to the inclusion of highly excited vibrational states and therefore the choice of vibrational weights. Accurate knowledge of the target vibrational population is hence required to model experimental KER cross sections.

We have compared the KER cross sections for H_2^+, D_2^+, and T_2^+ and demonstrated that the results for all three molecules are similar except in the low-E_k region, where the different populations of highly excited vibrational states have a strong effect. Surprisingly, our H_2^+ KER results are in better agreement with the measurements of El Ghazaly *et al.* [18] than the D_2^+ results, which still showed reasonable agreement at $E_{in} = 100$ eV. Measurements of the T_2^+ KER cross sections are not available, but the good agreement of our H_2^+ and D_2^+ results with experiment suggest that our T_2^+ calculations are similarly accurate.

The theoretical techniques utilized in the present work can be applied to study the KER processes of other molecules. Of particular interest are those of relevance to the modeling of fusion and industrial plasmas. Recently the molecular CCC method was successfully applied to study the elastic, excitation and ionization processes in e-H_2 scattering [33]. The study of KER processes in electron-impact dissociation of H_2 is the natural next step for this project.

ACKNOWLEDGMENTS

We would like to thank Dr. James Colgan for reviewing this manuscript and Prof. L. Wolniewicz, Prof. Defrance, and Dr. El Ghazaly for sending us their data in electronic form. This work was undertaken with support from the Australian Research Council and Curtin University, the assistance of resources from the National Computational Infrastructure, and resources and a student internship for L.H.S. from the Pawsey Supercomputing Centre, with funding from the Australian Government and Government of Western Australia. M.C.Z. would like to specifically acknowledge Los Alamos National Laboratory's (LANL's) ASC PEM Atomic Physics Project for its support. The LANL is operated by Los Alamos National Security, LLC for the National Nuclear Security Administration of the US Department of Energy under Contract No. DEAC52-06NA25396.

[1] R. K. Janev, At. Plasma-Mater. Interact. Data Fusion **9**, 1 (2001).
[2] S. Matt, T. Fiegele, G. Senn, K. Becker, H. Deutsch, O. Echt, A. Stamatovic, P. Scheier, and T. D. Märk, At. Plasma-Mater. Interact. Data Fusion **9**, 11 (2001).
[3] L. Sanche, Eur. Phys. J. D **35**, 367 (2005).
[4] M. Inokuti and M. J. Berger, Nucl. Instrum. Methods Phys. Res. Sect. B **27**, 249 (1987).
[5] M. Inokuti, M. A. Dillon, and M. Kimura, Int. J. Quantum Chem. **32**, 251 (1987).
[6] M. J. Berger and L. Paul, *Atomic and Molecular Data for Radiotherapy and Radiation Research* (International Atomic Energy Agency, Vienna, 1995), Chap. 7.
[7] J. L. Fox, M. I. Galand, and R. E. Johnson, Space Sci. Rev. **139**, 3 (2008).
[8] J. Lecointre, J. J. Jureta, J. B. A. Mitchell, V. Ngassam, A. E. Orel, and P. Defrance, J. Phys. B **41**, 045201 (2008).
[9] J. Lecointre, S. Cherkani-Hassani, D. S. Belic, J. J. Jureta, K. Becker, H. Deutsch, T. D. Märk, M. Probst, R. K. Janev, and P. Defrance, J. Phys. B **40**, 2201 (2007).
[10] J. Lecointre, D. S. Belic, J. J. Jureta, K. Becker, H. Deutsch, J. Limtrakul, T. D. Märk, M. Probst, and P. Defrance, J. Phys. B **40**, 85 (2007).
[11] H. Cherkani-Hassani, D. S. Belic, J. J. Jureta, and P. Defrance, J. Phys. B **39**, 5105 (2006).
[12] J. Lecointre, D. S. Belic, H. Cherkani-Hassani, J. J. Jureta, and P. Defrance, J. Phys. B **39**, 3275 (2006).
[13] E. M. Bahati, J. J. Jureta, D. S. Belic, S. Rachafi, and P. Defrance, J. Phys. B **34**, 1757 (2001).
[14] E. M. Bahati, J. J. Jureta, D. S. Belic, H. Cherkani-Hassani, M. O. Abdellahi, and P. Defrance, J. Phys. B **34**, 2963 (2001).
[15] E. M. Bahati, J. J. Jureta, H. Cherkani-Hassani, and P. Defrance, J. Phys. B **34**, L333 (2001).
[16] J. Lecointre, J. J. Jureta, and P. Defrance, J. Phys. B **43**, 105202 (2010).
[17] J. Lecointre, M. O. A. El Ghazaly, J. J. Jureta, D. S. Belic, X. Urbain, and P. Defrance, J. Phys. B **42**, 075201 (2009).

[18] M. O. A. El Ghazaly, J. Jureta, X. Urbain, and P. Defrance, J. Phys. B **37**, 2467 (2004).
[19] Z. Amitay, A. Baer, M. Dahan, L. Knoll, M. Lange, J. Levin, I. F. Schneider, D. Schwalm, A. Suzor-Weiner, Z. Vager, R. Wester, A. Wolf, and D. Zajfman, Science **281**, 75 (1998).
[20] D. Zajfman and Z. Amitay, Phys. Rev. A **52**, 839 (1995).
[21] T. Weber *et al.*, Nature (London) **431**, 437 (2004).
[22] L. P. H. Schmidt, T. Jahnke, A. Czasch, M. Schöffler, H. Schmidt-Böcking, and R. Dörner, Phys. Rev. Lett. **108**, 073202 (2012).
[23] D. T. Stibbe and J. Tennyson, New J. Phys. **1**, 2 (1998).
[24] M. C. Zammit, D. V. Fursa, J. S. Savage, I. Bray, L. Chiari, A. Zecca, and M. J. Brunger, Phys. Rev. A **95**, 022707 (2017).
[25] G. H. Dunn, Phys. Rev. **172**, 1 (1968).
[26] J. M. Peek, Phys. Rev. **134**, A877 (1964).
[27] D. E. Ramaker and J. M. Peek, At. Data **5**, 167 (1973).
[28] M. C. Zammit, D. V. Fursa, and I. Bray, Phys. Rev. A **90**, 022711 (2014).
[29] M. C. Zammit, D. V. Fursa, and I. Bray, Phys. Rev. A **88**, 062709 (2013).
[30] M. C. Zammit, D. V. Fursa, J. S. Savage, and I. Bray, J. Phys. B **50**, 123001 (2017).
[31] N. F. Lane, Rev. Mod. Phys. **52**, 29 (1980).
[32] W. A. Isaacs and M. A. Morrison, Phys. Rev. A **53**, 4215 (1996).
[33] M. C. Zammit, J. S. Savage, D. V. Fursa, and I. Bray, Phys. Rev. A **95**, 022708 (2017).
[34] D. F. Dance, M. F. A. Harrison, R. D. Rundel, and A. C. H. Smith, Proc. Phys. Soc. **92**, 577 (1967).
[35] G. H. Dunn and B. Van Zyl, Phys. Rev. **154**, 40 (1967).
[36] J. M. Peek, Phys. Rev. A **10**, 539 (1974).
[37] J. S. Savage, D. V. Fursa, M. C. Zammit, and I. Bray, J. Phys.: Conf. Ser. **488**, 052016 (2014).
[38] L. Wolniewicz and J. Poll, J. Mol. Spectrosc. **72**, 264 (1978).
[39] E. Gislason, J. Chem. Phys. **58**, 3702 (1973).
[40] F. von Busch and G. H. Dunn, Phys. Rev. A **5**, 1726 (1972).
[41] D. Wünderlich and U. Fantz, At. Data Nucl. Data Tables **97**, 152 (2011).
[42] B. Peart and K. T. Dolder, J. Phys. B **6**, 2409 (1973).
[43] G. H. Dunn, B. Van Zyl, and R. N. Zare, Phys. Rev. Lett. **15**, 610 (1965).
[44] D. Mathur, J. B. Hasted, and S. U. Khan, J. Phys. B **12**, 2043 (1979).
[45] R. Caudano and J. M. Delfosse, J. Phys. B **1**, 813 (1968).